Published in final edited form as:

J Pharm Sci. 2014 January ; 103(1): . doi:10.1002/jps.23765.

CYP1A1 and CYP1B1-mediated biotransformation of the antitrypanosomal methamidoxime prodrug DB844 forms novel metabolites through intramolecular rearrangement

Wujian Ju[1], **Sihyung Yang**[1], **John H. Ansede**[2], **Chad E. Stephens**[3], **Arlene S. Bridges**[4], **Robert D. Voyksner**[5], **Mohamed A. Ismail**[6], **David W. Boykin**[6], **Richard R. Tidwell**[4], **James Edwin Hall**[4], and **Michael Zhuo Wang**[1,†]

[1]Department of Pharmaceutical Chemistry, School of Pharmacy, The University of Kansas, Lawrence, KS, USA

[2]Parion Sciences, Durham, NC, USA

[3]Department of Chemistry and Physics, Georgia Regents University, Augusta, GA, USA

[4]Department of Pathology and Laboratory Medicine, School of Medicine, The University of North Carolina at Chapel Hill, Chapel Hill, NC, USA

[5]LCMS Limited, Durham, NC, USA

[6]Department of Chemistry, Georgia State University, Atlanta, GA, USA

Abstract

DB844 (CPD-594-12), *N*-methoxy-6-{5-[4-(*N*-methoxyamidino)phenyl]-furan-2-yl}-nicotinamidine, is an oral prodrug that has shown promising efficacy in both mouse and monkey models of second stage human African trypanosomiasis. However, gastrointestinal (GI) toxicity was observed with high doses in a vervet monkey safety study. In the current study, we compared the metabolism of DB844 by hepatic and extrahepatic cytochrome P450s to determine if differences in metabolite formation underlie the observed GI toxicity. DB844 undergoes sequential *O*-demethylation and *N*-dehydroxylation in the liver to form the active compound DB820 (CPD-593-12). However, extrahepatic CYP1A1 and CYP1B1 produced two new metabolites, MX and MY. Accurate mass and collision-induced dissociation mass spectrometry analyses of the metabolites supported proposed structures of MX and MY. In addition, MY was confirmed with a synthetic standard and detection of nitric oxide release when DB844 was incubated with CYP1A1. Taken altogether, we propose that MX is formed by insertion of an oxygen into the amidine C=N to form an oxaziridine, which is followed by intramolecular rearrangement of the adjacent *O*-methyl group and subsequent release of nitric oxide. The resulting imine ester, MX, is further hydrolyzed to form MY. These findings may contribute to furthering the understanding of toxicities associated with benzamidoxime- and benzmethamidoxime-containing molecules.

Keywords

CYP1A1; CYP1B1; cytochrome P450; intramolecular rearrangement; drug metabolism; prodrugs; human African trypanosomiasis; metabolite identification; nitric oxide

[†]**Corresponding Author:** Michael Zhuo Wang, Ph.D. (Telephone: +785 864 1899; Fax: +785 864 5736; michael.wang@ku.edu).

Conflict of Interest Statement: The authors declare no conflict of interest.

INTRODUCTION

Human African trypanosomiasis (HAT; or sleeping sickness), a parasitic infection, is fatal if left untreated.[1] During the first stage of HAT, *Trypanosoma brucei*(*T. b.*)*gambiense* and *T. b. rhodesiense* are confined to the hemolymphatic system. The disease progresses to second stage when parasites cross the blood-brain barrier and invade the central nervous system (CNS), leading to the deterioration of neurological function and disruption of the sleep/wake cycle, hence the name “sleeping sickness”. Drugs currently used to treat HAT suffer from poor oral bioavailability and thus require intravenous or intramuscular administration. Reliance on injectable medications, as well as equipped medical facilities to administer the medications, makes it difficult to treat patients in rural Africa where HAT is endemic.[2] In addition, many of these drugs cause moderate to severe adverse effects. Melarsoprol, for example, which is used to treat second stage HAT, causes fatal reactive encephalopathy in up to 12% of treated patients.[3] As a result, there is an urgent need to develop safer and orally active drugs to treat HAT, especially second stage HAT.

Pentamidine is an effective first stage HAT treatment, but must be administered intramuscularly to overcome low oral bioavailability. Due to minimal blood-brain barrier permeability, it is not curative against second stage HAT.[4] To enhance the oral bioavailability of pentamidine and other amidine analogs, a prodrug approach has been employed. The prodrug pafuramidine (DB289) was synthesized by methoxylating the two amidine moieties of furamidine (DB75), a pentamidine analog.[5–7] Pafuramidine exhibited 85-fold greater permeability across Caco-2 cell monolayers than furamidine.[8] In addition, it was biotransformed to the active compound DB75 in the liver and intestine *via* sequential *O*-demethylation and *N*-dehydroxylation, reactions predominantly catalyzed by cytochrome P450 (CYP) enzymes and cytochrome b_5/NADH-cytochrome b_5 reductase, respectively.[9–12] Pafuramidine administered orally achieved an 89% cure rate against first stage HAT in a phase III clinical trial; however, its development was later terminated due to unexpected, delayed severe kidney injury in an expanded phase I safety trial.[13]

In an effort to discover orally active trypanocides for the treatment of second stage HAT, an aza-analog of furamidine, DB820 (6-[5-(4-amidinophenyl)-furan-2-yl]nicotinamidine; CPD-593-12) (Figure 1), and its methoxy prodrug, DB844 (*N*-methoxy-6-{5-[4-(*N*-methoxyamidino)phenyl]-furan-2-yl}-nicotinamidine; CPD-594-12) (Figure 1), were synthesized and their potential to treat second stage HAT tested. DB844 was relatively inactive against trypanosomes, exhibiting an *in vitro* IC_{50} of 37 μM against *T. b. rhodesiense* STIB900, thus indicating that biotransformation to the active compound DB820, a potent trypanocide exhibiting an *in vitro* IC_{50} of 5.2–7.0 nM, is required.[14,15] The biotransformation of DB844 to DB820 occurs in the liver and involves sequential *O*-demethylation and *N*-dehydroxylation[16], similar to the biotransformation of pafuramidine. DB844 administered orally was 100% curative in the chronic CNS (*T. b. brucei* GVR35) mouse model, which mimics second stage HAT, but only approximately 40% (3/7 monkeys) curative in the second stage HAT (*T. b. rhodesiense* KETRI 2537) vervet monkey model.[15,17] After the 14th daily oral dose of DB844 at 6 mg/kg in vervet monkeys, the geometric mean (90% CI) maximum plasma concentration and terminal half-life of DB844 were 0.43 μM (0.1, 1.8 μM) and 0.24 day (0.14, 0.40 day), respectively.[17] In the safety portion of the vervet monkey study, higher oral DB844 doses (10 and 20 mg/kg body weight daily for 10 days) elicited marked gastrointestinal (GI) abnormalities (ulceration and inflammation), which were not observed with other methoxyamidine prodrugs (*e.g.*, pafuramidine[18] and DB868[19]). To determine why DB844 caused GI toxicity, we examined DB844 metabolism by hepatic and extrahepatic CYP enzymes, as well as liver and intestinal microsomes from monkeys and humans, subsequently identifying two novel metabolites formed by extrahepatic CYP1A1 and CYP1B1, MX and MY. We have proposed herein a

metabolic pathway involving intramolecular rearrangement and nitric oxide release that led to the formation of MX and MY. These results may contribute to the understanding of DB844-mediated GI toxicity, as well as the toxicities of other methoxyamidine-containing molecules.

MATERIALS AND METHODS

Materials

DB844, DB820, M1A (DB1284), M1B (DB1058), M2A (DB1285), M2B (DB1212), M3 (DB821), and deuterium-labeled DB844 analogs (Figure 1) were synthesized as previously reported.[14,20] Supersomes™, microsomes prepared from baculovirus-infected insect cells expressing human CYP enzymes and NADPH-cytochrome P450 reductase, were purchased from BD Biosciences (San Jose, CA). However, CYP2J2, CYP4F2, CYP4F3A, CYP4F3B, and CYP4F12 Supersomes™ coexpressed both NADPH-cytochrome P450 reductase and cytochrome b_5. Corresponding control microsomes, prepared from insect cells infected with either wild-type baculovirus or baculovirus containing cDNA-expressed human NADPH-cytochrome P450 reductase and cytochrome b_5, also were obtained from BD Biosciences. *Escherichia coli*(*E. coli*) expressing human CYP1A1 and NADPH-cytochrome P450 reductase were custom prepared by Cypex, Ltd. (Dundee, Scotland, UK). Human liver microsomes (HLM; mixed gender, pool of 200), human intestinal microsomes (HIM; mixed gender, pool of 13), liver microsomes from cynomolgus monkeys treated with saline (cynoLM-saline; male, pool of 3) or β-naphthoflavone (cynoLM-β-NF; male, pool of 4), vervet monkey liver microsomes (vervet LM; male, custom-prepared) and vervet monkey intestinal microsomes (vervet IM; male, custom-prepared) were purchased from XenoTech LLC (Lenexa, KS). CynoLM-β-NF was reported by the vendor to have 8-fold higher 7-ethoxyresorufin *O*-dealkylation (EROD) activity (2370 pmol/mg protein/min) than the control cynoLM-saline. (4-Methoxycarbonylphenyl)boronic acid was obtained from Combi-Blocks, Inc. (San Diego, CA). Ammonium formate, formic acid, trifluoroacetic acid (TFA), β-NADPH, acetonitrile (HPLC-grade), water (HPLC-grade), and all other chemicals were purchased from Sigma-Aldrich (St. Louis, MO) or Fisher Scientific (Pittsburgh, PA).

Metabolism of DB844 by Recombinant Human CYP Enzymes

The metabolism of DB844 by recombinant human CYP enzymes (1A1, 1B1, 1A2, 2C8, 2C9, 2C19, 2D6, 2J2, 3A4, 4F2, 4F3A, 4F3B and 4F12) was studied using a method previously published for pafuramidine.[10] Briefly, incubation mixtures (in triplicate) contained DB844 (3 μM final concentration), recombinant CYP enzymes individually (50 pmol/mL), 100 mM phosphate buffer (pH 7.4), and 3.3 mM $MgCl_2$. Reactions were initiated by the addition of NADPH (1 mM final concentration) and allowed to proceed for 15 min at 37°C. Control incubations were conducted with control Supersomes™ (0.25 mg/mL) or in the absence of NADPH. The reactions were stopped with half volume of ice-cold acetonitrile containing 0.1% (v/v) formic acid. After centrifugation to pellet precipitated proteins, the supernatants were analyzed by HPLC/UV and the % substrate consumed (instead of metabolite formation) was calculated as sequential reactions occurred during the 15-min incubation. Recombinant CYP enzyme concentration and incubation time were chosen to allow formation of primary and secondary metabolites before the complete disappearance of the substrate.

Reactions for metabolite identification studies were conducted with sample preparation and conditions similar to those described above, except that recombinant CYP enzymes were added to give a final concentration of 10 pmol/mL for CYP1A1 (enzyme concentration was lowered due to greater efficiency in metabolizing DB844) or 50 pmol/mL for CYPs 1B1 and 1A2. Samples that utilized deuterium-labeled analogs were concentrated 20-fold using

Empore C18-SD SPE cartridges (Sigma-Aldrich). After loading the quenched reaction mixture (2 mL), the membrane was washed five times with HPLC-grade water (1 mL). The concentrated sample was eluted with acetonitrile (0.1 mL) and immediately dried under nitrogen. The dried sample was reconstituted with 0.1 mL of 8% (v/v) acetonitrile containing 35 mM formic acid and 15 mM ammonium formate prior to HPLC/UV and HPLC/MS analyses.

Metabolism of DB844 by liver and intestinal microsomes

The metabolism of DB844 by liver and intestinal microsomes from humans and monkeys was studied using a similar method as described above. Briefly, incubation mixtures (in triplicate) contained DB844 (10 μM final concentration), 100 mM phosphate buffer (pH 7.4), and 3.3 mM MgCl2, and microsomes (1.0 mg/mL). Higher microsomal protein concentrations were not tested due to limited microsomal stock concentrations, especially for intestinal microsomes. Reactions were initiated by the addition of NADPH (1 mM final concentration) and allowed to proceed for up to 30 min at 37°C. The reactions were stopped with half volume of ice-cold acetonitrile at 0, 10, 20, and 30 min. After centrifugation to pellet precipitated proteins, the supernatants were analyzed by HPLC/UV and DB844 metabolites were identified by comparing retention times to those of synthetic standards. A positive control incubation with recombinant CYP1A1 (50 pmol/mg) was performed and analyzed in parallel.

Biosynthesis of MX and MY

Cultures of *E. coli* expressing human CYP1A1 and NADPH-cytochrome P450 reductase were used for the biosynthesis of the metabolites MX and MY for structural elucidation. DB844 (25 μM final concentration) was added to a suspension of *E. coli* (200 pmol CYP1A1/mL; 2 L per reaction) and the mixture incubated at 37°C for 30 min. Following centrifugation at 13,000 rpm for 1 min to pellet the bacteria and terminate the reaction, the supernatant was removed, mixed with an equal volume of acetonitrile and placed on ice. Ten min later, the sample was centrifuged at 16,000 *g* for 1 min to pellet precipitated proteins. The resulting supernatant (crude mixture) was stored in 50-mL aliquots at −80°C. To purify MX and MY, the crude mixture (100 mL) was concentrated using Empore C18-SD SPE cartridges. After loading the sample, the membrane was washed five times with HPLC-grade water (1 mL) prior to elution of the concentrated sample with acetonitrile (0.5 mL). The eluate was immediately dried under nitrogen and the remaining pellet stored at −80°C. Prior to HPLC separation, the pellet was reconstituted with 0.5 mL of 8% (v/v) acetonitrile containing 35 mM formic acid and 15 mM ammonium formate. MX and MY were separated from the concentrated sample (0.4 mL) on a custom-packed semi-preparative HPLC column (Zorbax Bonus-RP, 9.4 mm × 250 mm, 5 μm; Agilent, Santa Clara, CA) using a Varian ProStar Prep HPLC System (Palo Alto, CA). Mobile phase (A) consisted of HPLC-grade water with 35 mM formic acid and 15 mM ammonium formate; (B) consisted of 80:20 (v/v) acetonitrile:HPLC-grade water with 35 mM formic acid and 15 mM ammonium formate. The initial gradient condition was 10% B at a flow rate of 4 mL/min. Mobile phase B increased linearly to 60% over 25 min and then to 100% over 3 additional min. After washing with 100% B for 5 min, the system was re-equilibrated for 6 min with 10% B. UV absorbance was monitored at 359 nm and the eluent collected in 30-second fractions using a fraction collector. MX, M1A, and M1B eluted at approximately 14.4, 15.5, and 13.6 min, respectively. Fractions that contained MX were further concentrated using Empore C18-SD SPE cartridges. The final concentrated sample was reconstituted in 0.1 mL of 50% (v/v) acetonitrile prior to storage at −80°C. MY was obtained by allowing a portion of purified MX to hydrolyze under aqueous conditions.

Chemical Synthesis of the Proposed MY Metabolite

To synthesize the proposed MY metabolite, a mixture of 2-bromo-5-(4-methoxyamidino-2-pyridyl)furan (296 mg, 1.0 mmol; prepared as previously described[14]), (4-methoxycarbonylphenyl)boronic acid (200 mg, 1.1 mmol), palladium acetate (10 mg, 4.5 mol%), and powdered potassium phosphate (420 mg, 2.0 mmol) in methanol (12 mL) was stirred at room temperature under nitrogen for 3 h. The mixture was diluted with water to give a green precipitate. The precipitate was filtered and washed with water. Recrystallization from methanol (~200 mL, with concentration to ~50 mL) at room temperature overnight gave orange/tan crystals (114 mg, 32 mol%; mp 231–234°C). IR (cm^{-1}): 3433, 3318, 3169, 2992, 2957, 2937, 2900, 2819, 1706, 1628, 1600, 1276, 1052, 1025, 912, 858, 796, 765, 695. ^{1}H-NMR (DMSO-d_6): 3.78 (s, 3H), 3.86 (s, 3H), 6.29 (br s, NH_2), 7.32 (d, J = 3.6Hz, 1H), 7.36 (d, J = 3.6Hz, 1H), 7.93–8.11 (m, 6H), 8.86 (m, 1H). ^{13}C-NMR (DMSO-d_6): 52.2, 60.8, 111.1, 112.1, 118.0, 123.8, 126.8, 128.4, 129.9, 133.8, 134.2, 147.0, 148.3, 149.0, 152.9, 153.3, 165.8. Analytical calculated for $C_{19}H_{17}N_3O_4$•0.1CH_3OH (MW 354.56 g/mol): C, 64.70; H, 4.95; N, 11.85. Observed: C, 64.61; H, 4.89; N, 11.61.

HPLC/UV Analysis

DB844 and its metabolites were separated on an Agilent ZORBAX Bonus-RP analytical column (2.1 × 50 mm, 3.5 μm) at room temperature using an Agilent 1100 Series HPLC system equipped with a UV diode array detector. Mobile phase (A) consisted of HPLC-grade water with 35 mM formic acid and 15 mM ammonium formate; (B) consisted of 80:20 (v/v) acetonitrile:HPLC-grade water with 35 mM formic acid and 15 mM ammonium formate. For HPLC/UV analysis of microsomal samples, the initial gradient condition was 5% B at a flow rate of 0.35 mL/min. Mobile phase B increased linearly to 80% over 15 min and then the column was washed with 95% B for 1 min. The system was re-equilibrated for 6 min with 5% B with a total run time of 22 min. For HPLC/UV analysis of purified MX and MY, the initial gradient condition was 10% B at a flow rate of 0.35 mL/min. Mobile phase B increased linearly to 100% over 25 min. The system was re-equilibrated for 6 min with 10% B prior to the next injection. All samples were monitored at a UV absorbance of 359 nm.

HPLC/MS Analyses

Initial qualitative characterization of DB844 metabolites and synthetic standards employed an Agilent 1100 Series HPLC system equipped with a UV detector and coupled to an MSD ion trap mass spectrometer (HPLC/ion trap MS; Agilent) as previously described.[16] Samples were separated on an Agilent ZORBAX Bonus-RP analytical column (2.1 × 150 mm, 5 μm) at room temperature. Mobile phase (C) consisted of HPLC-grade water with 0.025% (v/v) TFA; (D) consisted of 80:20 (v/v) acetonitrile:HPLC-grade water with 0.025% (v/v) TFA. The initial gradient condition was 10% D at a flow rate of 0.35 mL/min. Mobile phase D increased linearly to 60% over 25 min and then to 100% over 3 additional min. After washing with 100% D for 5 min, the system was re-equilibrated for 6 min with 10% D. UV absorbance was monitored at 359 nm prior to introduction into a pneumatically assisted electrospray (ESI) interface operated in positive mode. Full-scan MS (molecular ion) and auto MS/MS (MS^2 and MS^3 product ions) mass spectra were acquired on the ion trap mass spectrometer using previously described instrument parameters.[16]

Accurate mass analysis was performed on an Agilent 6530 Accurate-Mass Quadrupole Time-of-Flight (Q-TOF) LC/MS (HPLC/Q-TOF) to confirm the molecular formula and MS/MS product ion elemental compositions. Samples were initially separated on an Agilent 1290 HPLC system with conditions similar to those described above for the HPLC/ion trap MS work. Prior to analysis, the Q-TOF mass resolution, sensitivity and mass calibration

were checked with the Agilent tune compound. The reference liquid was introduced into the Q-TOF by an Agilent isocratic pump running at 0.7 mL/min with a 1:100 split, resulting in a 7 μL/min flow rate into the dual ESI source. Parameters for the ESI dual source were: drying gas, 9 L/min of nitrogen; nebulization gas, 30 psi; sheath gas flow rate, 11 L/min; sheath gas temperature, 350°C; drying gas temperature, 350°C; capillary voltage, 4000 V; nozzle voltage, 1000 V; fragmentor voltage, 110 V; and CID collision gas, nitrogen. The instrument was operated in auto MS/MS mode, scanning *m/z* 100–1000 using positive ion detection. MS/MS spectra were acquired at collision energies of 10, 20, 40 and 60 V. The Agilent tuning ions of *m/z* 121.05087 and *m/z* 922.00980 served as reference masses for exact mass determination. The resulting data were processed using Agilent MassHunter Qualitative analysis workstation software (version B.05).

Nitrate/Nitrite Formation Assay

The nitrate/nitrite fluorometric assay (Cayman Chemical Co., Ann Arbor, MI) was used to quantify nitric oxide (NO) formation. NO has a very short half-life in biological systems, as it is rapidly scavenged/oxidized to form the end-products nitrate and nitrite. To measure NO formation following DB844 metabolism, DB844 (10 μM final concentration; in triplicate) was incubated with recombinant CYP enzymes (CYP1A1, CYP1A2 or CYP1B1 at 50 pmol/mL) or control Supersomes™ (0.25 mg/mL) for 1 h as described under *Metabolism of DB844 by Recombinant Human CYP Enzymes* in *Materials and Methods*. Control incubations were conducted with heat-inactivated enzymes (90°C for 5 min prior to addition of DB844 and β-NADPH) or in the absence of recombinant CYP enzyme or DB844. Reactions were stopped by heating the samples at 90°C for 5 min. The reaction mixtures were transferred to Amicon Ultra-0.5 Centrifugal Filters with Ultracell-30 membrane (EMD Millipore, Billerica, MA) and centrifuged at 14,000 *g* for 30 min to remove proteins. The resulting filtrate was dried under vacuum using a CentriVap concentrator (Labconco Corp., Kansas City, MO) and reconstituted with the assay buffer provided in the kit. The assay was performed according to the manufacturer's protocol. Briefly, nitrate in the sample was reduced to nitrite with nitrate reductase. Subsequent addition of 2,3-diaminonaphthalene (DAN) resulted in the formation of 1(H)-naphthotriazole, the fluorescent product. Sodium hydroxide was added to enhance the fluorescence of the final product. Samples were measured at an excitation wavelength of 360 nm and an emission wavelength of 404 nm, which had been optimized for minimal background signal from DB844 and β-NADPH. A series of nitrite standard solutions (0.078–5.0 μM) were prepared for calibration curves.

Data Analysis

The percent substrate consumed in DB844 incubations with recombinant CYP enzymes was determined after normalizing DB844 concentrations in these reactions to that in incubations with control Supersomes™ (expressed as 0% substrate consumed) at 15 min. Differences in average nitrate/nitrite concentrations between incubations with recombinant CYP enzymes or control Supersomes™ and with heat-inactivated enzymes (negative controls) were determined using unpaired, two-tailed Student's *t*-tests (GraphPad Prism 5.04; GraphPad Software, Inc., La Jolla, CA). Statistical outcomes were considered significant when the *p*-value was <0.05.

RESULTS

Metabolism of DB844 by Recombinant Human CYP Enzymes

A panel of recombinant human CYP enzymes, comprised of hepatically and extrahepatically expressed CYPs, was used to evaluate the metabolism of DB844 by individual CYP isoforms. Activity was determined as the percent of substrate (DB844) consumed/depleted during a 15-min incubation. DB844 was metabolized by multiple human CYPs in NADPH-

dependent reactions (Figure 2; data not shown for NADPH-deficient reactions). CYP2J2 exhibited the greatest activity (96%), followed by CYP1A1 (90%), CYP1A2 (42%), CYP4F2 (39%), CYP1B1 (30%), CYP4F3B (19%) and CYP3A4 (16%). The remaining CYPs, 2C8, 2C9, 2C19, 2D6, 4F3A and 4F12, only showed marginal activity (<5% substrate depletion). Neither control microsomes prepared from empty baculovirus-infected insect cells nor from baculovirus-infected insect cells expressing NADPH-cytochrome P450 reductase and cytochrome b_5 could metabolize DB844 (data not shown).

Incubation of DB844 (*m/z* 366.2) with hepatic CYP enzymes (*i.e.*, CYPs 1A2, 3A4, 2J2, 4F2 and 4F3B) resulted in the expected *O*-demethylation metabolites, M1A (*m/z* 352.2), M1B (*m/z* 352.2) and M3 (*m/z* 338.2; from double *O*-demethylation), as identified by comparison of HPLC retention times and MS/MS fragmentation patterns to those of synthetic standards. A representative HPLC/UV chromatogram from an incubation with CYP1A2 is shown in Figure 3A. These *O*-demethylation metabolites are the same as those detected when DB844 was incubated with HLM.[16] However, the *N*-dehydroxylation metabolites formed in HLM (*e.g.*, M2A and M2B which elute between M3 and M1B; Figure 4A) were not observed in incubations with the recombinant human CYP enzymes (Figure 3A), presumably because the Supersomes™ used in the current studies lacked NADH-cytochrome b_5 reductase expression.[11,21]

Incubation of DB844 with the extrahepatic enzymes CYP1A1 and CYP1B1 resulted in two novel metabolites, MX and MY (Figures 3B and 3C, respectively). HPLC/ion trap MS analysis revealed that MX had a molecular ion of *m/z* 351.2, suggesting a loss of NH (15 Da) from DB844 (*m/z* 366.2) rather than the loss of CH_2 (14 Da) that results in M1A (*m/z* 352.2) and M1B (*m/z* 352.2). Initial HPLC/ion trap MS analysis was unable to provide parent ion information for MY due to low abundance and high background noise.

Metabolism of DB844 by liver and intestinal microsomes from humans and monkeys

To determine metabolite profiles of DB844 in liver and intestinal microsomes from humans and monkeys, incubation mixtures were analyzed by HPLC/UV and representative chromatograms for 30-min incubations are shown in Figure 4. Pooled HLM, pooled HIM, vervet LM and vervet IM produced similar metabolite profiles (Figures 4A–D), consisting of primary *O*-demethylation metabolites (M1A and M1B), secondary *N*-dehydroxylation metabolites (M2A and M2B), and double *O*-demethylation metabolite (M3). Neither MX nor MY was detected in these reactions (data for shorter incubations are not shown). However, when liver microsomes prepared from β-NF-treated cynomolgus monkeys were used, MX and MY were generated in DB844 incubations (Figure 4E). In contrast, neither MX nor MY was detected in incubations with saline-treated cynomolgus liver microsomes (data for shorter incubations are not shown) (Figure 4F). In positive control incubation with recombinant CYP1A1, MX and MY eluted at 7.6 and 11.6 min, respectively (data not shown).

Biosynthesis and Characterization of MX and MY

In order to determine more detailed structural information for the novel metabolites, MX and MY were purified from incubations of DB844 with *E. coli* expressing CYP1A1. MX was unstable and converted to MY during both the concentration/purification process and in the reconstitution solvent (50% (v/v) acetonitrile). This was evidenced by 1) the detection of MY in semi-preparative HPLC fractions that were expected to only contain MX due to good HPLC separation between MX and MY (14.4 *vs.* 28.2 min; Figure 5) and 2) the MX peak in the HPLC/UV chromatogram decreased following a 6-h incubation in reconstitution solvent at room temperature while the MY peak increased (Figure 5). These results indicate that MX is not chemically stable and degrades to MY.

The accurate masses (and formulae) of MX and MY were determined to be 350.1377 Da ($C_{19}H_{18}N_4O_3$) and 351.1229 Da ($C_{19}H_{17}N_3O_4$), respectively. The molecular ion clusters of MX and MY exhibited isotopic distributions matching those predicted (Figures 6A and 6C). Collision-induced dissociation (CID) fragmentation of the MX molecular ion $[MX+H]^+$ produced a predominant product ion with *m/z* 304.1086 ($C_{18}H_{14}N_3O_2$), corresponding to the loss of OCH_3NH_2 (loss of 47 Da) (Figure 6B). CID fragmentation of the MY molecular ion $[MY+H]^+$ produced a predominant product ion with *m/z* 305.0927 ($C_{18}H_{13}N_2O_3$), corresponding to the loss of OCH_3NH_2 (Figure 6D).

MS^2 and MS^3 Analyses of MX and MY

Purified MX and MY from biosynthesis and M1B synthetic standard were analyzed by HPLC-ion trap MS; the MS^2 and MS^3 mass spectra are presented in Figure 7. CID fragmentation of the M1B molecular ion $[M1B+H]^+$ (*m/z* 352.2) produced one major product ion with *m/z* 305.1, corresponding to the characteristic loss of OCH_3NH_2 (loss of 47 Da) from the methoxyamidine on the pyridine ring side, and two minor product ions with *m/z* 321.2 and *m/z* 335.1, corresponding to the loss of OCH_3 (loss of 31 Da) and NH_3 (loss of 17 Da), respectively (Figure 7A). The *m/z* 305.1 product ion underwent further CID fragmentation, resulting in several MS^3 product ions that included a major ion with *m/z* 288.0 (loss of NH_3 from the amidoxime side; 17 Da) and a minor ion with *m/z* 272.1 (loss of $OHNH_2$ from the phenyl ring amidoxime side; 33 Da).

$[MX+H]^+$ (*m/z* 351.2) was 1 Da less than $[M1B+H]^+$ (Figure 7B). CID fragmentation of $[MX+H]^+$ produced one major product ion with *m/z* 304.1, corresponding to the characteristic loss of OCH_3NH_2 from the methoxyamidine moiety. The *m/z* 304.1 product ion underwent further CID fragmentation, resulting in two major MS^3 product ions with *m/z* 289.0 (loss of CH_3; 15 Da) and *m/z* 272.0 (loss of $OHCH_3$; 32 Da).

$[MY+H]^+$ (*m/z* 352.2; Figure 7C) has the same molecular weight as M1A and M1B. CID fragmentation of $[MY+H]^+$ produced one major product ion with *m/z* 305.1, corresponding to the characteristic loss of OCH_3NH_2 from the methoxyamidine moiety. The *m/z* 305.1 product ion underwent further CID fragmentation, resulting in two major MS^3 product ions with *m/z* 273.0 (loss of $OHCH_3$; 32 Da) and *m/z* 245.0 (loss of 60 Da).

Determination of the Site of Metabolism using Deuterium-labeled DB844

To determine the site of metabolism that results in MX and MY formation, deuterium-labeled DB844 analogs (DB844-pyridyl-CD_3, DB844-phenyl-CD_3, and DB844-D_4; Figure 1) were individually incubated with recombinant CYP1A1. MX formed from DB844-pyridyl-CD_3 exhibited a molecular ion of *m/z* 354.1 in HPLC/ion trap MS analysis (Figure 8A). This is 3 Da greater than MX formed from unlabeled DB844 (Figure 7B), indicating that the three deuterium atoms on the pyridine side were retained in MX. CID fragmentation of the *m/z* 354.1 molecular ion generated a MS^2 product ion with *m/z* 303.9, corresponding to the characteristic loss of OCD_3NH_2 from the methoxyamidine on the pyridine ring side (loss of 50 Da). Further fragmentation of the *m/z* 303.9 ion produced several MS^3 product ions (*m/z* 288.8 and 271.8) similar to those produced from unlabeled MX. These results suggest that the methyl group on the pyridine ring side of DB844 remains intact in MX.

MX formed from DB844-phenyl-CD_3 exhibited a molecular ion of *m/z* 354.1 (Figure 8B), which is 3 Da greater than MX formed from unlabeled DB844, indicating that the three deuterium atoms on the phenyl side were retained in MX as well. CID fragmentation of the *m/z* 354.1 molecular ion gave rise to a major MS^2 product ion with *m/z* 307.0, corresponding to the characteristic loss of OCH_3NH_2 from the methoxyamidine on the pyridine ring side (loss of 47 Da). If such a loss had occurred from the methoxyamidine on the phenyl ring

side, it would have resulted in a loss of 50 Da (OCD_3NH_2), forming a product ion with *m/z* 304.1. This product ion was not detected, further confirming that the methyl group on the pyridine ring side of DB844 remains intact in MX. Further fragmentation of the *m/z* 307.0 ion produced two MS^3 product ions (*m/z* 288.9 and 271.9) similar to those generated from unlabeled DB844 (Figure 7B) and DB844-pyridyl-CD_3 (Figure 8A). These findings indicate that the loss of 18 Da (*m/z* 307.0 → 288.9) was due to the loss of CD_3, suggesting that the methyl group on the phenyl ring side of DB844 also remains in MX, but not as a methoxyamidine. This was further supported by HPLC/ion trap MS analysis of MY molecules formed from DB844-pyridyl-CD_3 and DB844-phenyl-CD_3 (data not shown).

Finally, HPLC/ion trap MS analysis of MX formed from DB844-D_4 (deuterated phenyl ring) showed a molecular ion of *m/z* 355.2 and a MS^2 product ion with *m/z* 308.1 (Figure 8C). These were 4 Da greater than the MX molecular ion and product ion formed from unlabeled DB844, indicating that the phenyl ring remains unaltered in MX.

Proposed Reaction Mechanism and Structures of MX and MY

Based on the HPLC/ion trap MS analysis of MX and MY described above, we have proposed a reaction mechanism for the formation of MX and MY from DB844 catalyzed by CYP1A1 and CYP1B1 (Scheme 1). CYP1A1 and CYP1B1 catalyze the insertion of oxygen into the C=N bond on the phenyl ring side of the molecule, forming an oxaziridine intermediate. Intramolecular rearrangement of the adjacent *O*-methyl bond follows and nitric oxide is subsequently released. The proposed intramolecular rearrangement of the adjacent *O*-methyl bond results in the formation of MX, an imine ester, which is further hydrolyzed to form the corresponding ester MY.

To support the proposed reaction mechanism and structures of MX and MY, an authentic MY standard was synthesized based on the proposed structure in Scheme 1. Synthetic MY eluted at the same time as purified MY from biosynthesis when analyzed by HPLC/ion trap MS (Figure 9A). CID fragmentation of synthetic MY produced a molecular ion of *m/z* 352.2 and one major MS^2 product ion with *m/z* 305.1. Further fragmentation produced several MS^3 product ions (*m/z* 273.0 and 245.0) (Figure 9B). This CID fragmentation pattern was similar to that exhibited by purified MY from biosynthesis under the same conditions (Figure 7C).

Nitric Oxide Formation

To further support the proposed reaction mechanism, the formation of nitric oxide was determined by quantifying the total amount of nitrate and nitrite present in incubations of DB844 with recombinant human CYP enzymes. Background signals were determined in incubations without the addition of CYP enzyme or DB844. Significant nitric oxide formation was detected in incubations with CYP1A1, but not with CYP1A2, CYP1B1 or control Supersomes, when compared to incubations with heat-inactivated enzymes (Figure 10).

DISCUSSION

DB844 is a novel oral prodrug that has shown promising efficacy in the mouse and monkey models of second stage HAT.[15,17] This compound undergoes complex biotransformation involving sequential *O*-demethylation and *N*-dehydroxylation reactions to form the active antitrypanosomal diamidine DB820 in HLM.[16] After oral administration of DB844 at a daily dose of 6 mg/kg in vervet monkeys, maximum plasma concentration of DB844 reached approximately 1–2 μM after the 14th dose and presumably even higher when 10 and 20 mg/kg daily doses were used in safety testing.[17] Hence DB844 substrate concentrations

(3 and 10 μM) used in this study are relevant to *in vivo* drug exposures. Human hepatic CYP enzymes, including CYPs 1A2, 2J2, 3A4, 4F2 and 4F3B, catalyzed the initial *O*-demethylation of DB844 to form M1A and M1B (Figure 2). These same enzymes also catalyzed the initial *O*-demethylation of pafuramidine (DB289) to form M1 (DB775) in the human liver.[10] Given the similarity between chemical structures of DB844 (Figure 1) and pafuramidine, it is presumed that CYP4F enzymes, as well as CYP3A4 and CYP1A2, play a predominant role in catalyzing the *O*-demethylation of DB844 in the human liver. Further reaction phenotyping studies employing selective chemical inhibitors, inhibitory antibodies, and correlation analysis are needed to confirm this.

In addition to catalyzing the *O*-demethylation of DB844, the extrahepatic CYP enzymes CYP1A1 and CYP1B1 generated two additional metabolites, MX and MY (Figure 3). These metabolites were not formed by hepatic CYP enzymes (*i.e.*, CYPs 1A2, 2J2, 3A4, 4F2 and 4F3B), explaining why neither was detected in incubations with HLM (Figure 4A). It was imperative to identify MX and MY since 1) it may help to assess the potential toxicity liability of these two metabolites in extrahepatic tissues that are known to express CYP1A1 and/or CYP1B1 (*e.g.*, small intestine[22] and lung[23]), and 2) it may serve as a marker reaction for CYP1A1 and CYP1B1 since CYP1A2 and other CYP enzymes examined in this study did not form MX or MY. Biosynthesized MX and MY, as well as authentic MY standard, were subsequently characterized using HPLC/ion trap MS fragmentation and HPLC/Q-TOF accurate mass analysis to elucidate their chemical structures. First, MX was found to be unstable and chemically degraded to MY. Second, there were clear differences between CID fragmentation patterns of MX, MY, and the *O*-demethylation metabolite M1B. Although similar fragmentation patterns were seen in the MS^2 mass spectra (*i.e.*, characteristic loss of OCH_3NH_2 (47 Da) from the methoxyamidine group), further fragmentation (MS^3) resulted in different product ions, loss of NH_3 (17 Da) from M1B, CH_3 radical (15 Da) from MX, and $HOCH_3$ (32 Da) from MY (Figure 7). Finally, the site at which DB844 is metabolized to form MX and MY was determined by employing deuterium-labeled DB844 analogs to probe potential reaction locations at the methyl group on the pyridine ring side, the methyl group on the phenyl ring side, and the phenyl ring (Figure 8). Our results suggest that both the methyl group on the phenyl ring side and on the pyridine ring side of DB844 were retained in MX. In addition, the methyl group on the phenyl ring side did not exist as methoxyamidine in MX. Upon consideration altogether, we have proposed an atypical CYP reaction mechanism that results in the formation of MX and MY from DB844 by CYP1A1 and CYP1B1 (Scheme 1). CYP1A1 and CYP1B1 introduce an oxygen atom into the amidine C=N bond of DB844, forming an oxaziridine intermediate. The intermediate undergoes intramolecular rearrangement of the adjacent *O*-methyl bond to produce MX, an imine ester, and release one molecule of nitric oxide. MX is further hydrolyzed in aqueous conditions to form the corresponding ester MY, which was confirmed using a synthetic standard based on the proposed MY structure (Figure 9). Furthermore, nitric oxide formation was detected in incubations of DB844 with recombinant CYP1A1 (Figure 10). In conclusion, our experimental evidence strongly supports the proposed reaction mechanism for CYP1A1/1B1-mediated MX and MY formation *via* intramolecular rearrangement (Scheme 1).

To evaluate if nitric oxide formation *via* conversion of DB844 to MX is a potential mechanism for the GI toxicity observed in DB844-treated vervet monkeys,[17] DB844 metabolite profiles were determined using liver and intestinal microsomes from monkeys and humans. Neither MX nor MY was detected in incubations with liver or intestinal microsomes from humans and vervet monkeys (Figures 4A–D), indicating that nitric oxide formation *via* conversion of DB844 to MX is unlikely a cause of the observed GI toxicity. However, both MX and MY were detected in liver microsomes prepared from β-NF-treated cynomolgus monkeys, but not from saline-treated control monkeys (Figures 4E and 4F). β-

NF is known to induce human CYP1A1 and CYP1A2.[24] Cynomolgus monkey CYP1A1 and CYP1A2 are highly homologous to human counterparts and CYP1A1 has been reported to be expressed in both cynomolgus monkey liver and intestine.[25,26] Thus, induction of cynomolgus monkey CYP1A1 likely explains the increased formation of MX in β-NF-treated cynomolgus liver microsomes. It would be interesting to examine if MX formation can be detected in β-NF-treated cynomolgus intestinal microsomes. Unfortunately, such intestinal microsomes were not available from the vendor. Taken together, nitric oxide formation *via* conversion of DB844 to MX may not explain the observed GI toxicity, but possibility exists where an elevated CYP1A1/1B1 due to induction (*e.g.*, by dietary phytochemicals[27]) leads to MX formation and nitric oxide release from DB844.

It is not yet known if this intramolecular rearrangement and resulting nitric oxide release can occur with other amidine analogs (*e.g.*, benzamidoximes/*N*-hydroxylated benzamidines). If true, it may contribute to the understanding of toxicity caused by other benzamidoxime- or benzmethamidoxime-containing molecules, such as ximelagatran, a direct thrombin inhibitor that failed in clinical trials due to idiosyncratic liver injury.[28]

Acknowledgments

This work was supported in part by a grant to the Consortium for Parasitic Drug Development (CPDD; http://www.thecpdd.org) from the Bill and Melinda Gates Foundation and by an NIH grant R01GM089994 (MZW). We would like to thank Michael P. Pritchard and Anna Kaaz from Cypex Limited for preparing the CYP1A1-expressing *E. coli*. We also would like to thank Dr. R. Scott Obach (Pfizer Inc., Groton, CT) for helpful discussion regarding the proposed reaction mechanism.

Abbreviations

CI	confidence interval
CID	collision-induced dissociation
CNS	central nervous system
CYP	cytochrome P450
EROD	7-ethoxyresorufin *O*-dealkylation
HAT	human African trypanosomiasis
HPLC	high performance liquid chromatography
MS	mass spectrometry
NO	nitric oxide
Q-TOF	quadrupole time-of-flight mass spectrometry
TFA	trifluoroacetic acid

References

1. Brun R, Blum J, Chappuis F, Burri C. Human African trypanosomiasis. Lancet. 2010; 375(9709): 148–159. [PubMed: 19833383]
2. Barrett MP, Boykin DW, Brun R, Tidwell RR. Human African trypanosomiasis: pharmacological re-engagement with a neglected disease. Br J Pharmacol. 2007; 152(8):1155–1171. [PubMed: 17618313]
3. Pepin J, Milord F. African trypanosomiasis and drug-induced encephalopathy: risk factors and pathogenesis. Trans R Soc Trop Med Hyg. 1991; 85(2):222–224. [PubMed: 1887477]
4. Sanderson L, Dogruel M, Rodgers J, De Koning HP, Thomas SA. Pentamidine movement across the murine blood-brain and blood-cerebrospinal fluid barriers: effect of trypanosome infection,

combination therapy, P-glycoprotein, and multidrug resistance-associated protein. J Pharmacol Exp Ther. 2009; 329(3):967–977. [PubMed: 19261919]

5. Das BP, Boykin DW. Synthesis and antiprotozoal activity of 2,5-bis(4-guanylphenyl)thiophenes and -pyrroles. J Med Chem. 1977; 20(9):1219–1221. [PubMed: 336890]
6. Steck EA, Kinnamon KE, Rane DS, Hanson WL. Leishmania donovani, Plasmodium berghei, Trypanosoma rhodesiense: antiprotozoal effects of some amidine types. Exp Parasitol. 1981; 52(3): 404–413. [PubMed: 7032963]
7. Steck EA, Kinnamon KE, Davidson DE Jr, Duxbury RE, Johnson AJ, Masters RE. Trypanosoma rhodesiense: evaluation of the antitrypanosomal action of 2,5-bis(4-guanylphenyl)furan dihydrochloride. Exp Parasitol. 1982; 53(1):133–144. [PubMed: 7056341]
8. Zhou L, Lee K, Thakker DR, Boykin DW, Tidwell RR, Hall JE. Enhanced permeability of the antimicrobial agent 2,5-bis(4-amidinophenyl)furan across Caco-2 cell monolayers via its methylamidoidme prodrug. Pharm Res. 2002; 19(11):1689–1695. [PubMed: 12458675]
9. Zhou L, Thakker DR, Voyksner RD, Anbazhagan M, Boykin DW, Hall JE, Tidwell RR. Metabolites of an orally active antimicrobial prodrug, 2,5-bis(4-amidinophenyl)furan-bis-O-methylamidoxime, identified by liquid chromatography/tandem mass spectrometry. J Mass Spectrom. 2004; 39(4):351–360. [PubMed: 15103648]
10. Wang MZ, Saulter JY, Usuki E, Cheung YL, Hall M, Bridges AS, Loewen G, Parkinson OT, Stephens CE, Allen JL, Zeldin DC, Boykin DW, Tidwell RR, Parkinson A, Paine MF, Hall JE. CYP4F enzymes are the major enzymes in human liver microsomes that catalyze the O-demethylation of the antiparasitic prodrug DB289 [2,5-bis(4-amidinophenyl)furan-bis-O-methylamidoxime]. Drug Metab Dispos. 2006; 34(12):1985–1994. [PubMed: 16997912]
11. Saulter JY, Kurian JR, Trepanier LA, Tidwell RR, Bridges AS, Boykin DW, Stephens CE, Anbazhagan M, Hall JE. Unusual dehydroxylation of antimicrobial amidoxime prodrugs by cytochrome b5 and NADH cytochrome b5 reductase. Drug Metab Dispos. 2005; 33(12):1886–1893. [PubMed: 16131524]
12. Wang MZ, Wu JQ, Bridges AS, Zeldin DC, Kornbluth S, Tidwell RR, Hall JE, Paine MF. Human enteric microsomal CYP4F enzymes O-demethylate the antiparasitic prodrug pafuramidine. Drug Metab Dispos. 2007; 35(11):2067–2075. [PubMed: 17709372]
13. Paine MF, Wang MZ, Generaux CN, Boykin DW, Wilson WD, De Koning HP, Olson CA, Pohlig G, Burri C, Brun R, Murilla GA, Thuita JK, Barrett MP, Tidwell RR. Diamidines for human African trypanosomiasis. Curr Opin Investig Drugs. 2010; 11(8):876–883.
14. Ismail MA, Brun R, Easterbrook JD, Tanious FA, Wilson WD, Boykin DW. Synthesis and antiprotozoal activity of aza-analogues of furamidine. J Med Chem. 2003; 46(22):4761–4769. [PubMed: 14561095]
15. Wenzler T, Boykin DW, Ismail MA, Hall JE, Tidwell RR, Brun R. New treatment option for second-stage African sleeping sickness: in vitro and in vivo efficacy of aza analogs of DB289. Antimicrob Agents Chemother. 2009; 53(10):4185–4192. [PubMed: 19620327]
16. Ansede JH, Voyksner RD, Ismail MA, Boykin DW, Tidwell RR, Hall JE. In vitro metabolism of an orally active O-methyl amidoxime prodrug for the treatment of CNS trypanosomiasis. Xenobiotica. 2005; 35(3):211–226. [PubMed: 16019947]
17. Thuita JK, Wang MZ, Kagira JM, Denton CL, Paine MF, Mdachi RE, Murilla GA, Ching S, Boykin DW, Tidwell RR, Hall JE, Brun R. Pharmacology of DB844, an orally active aza analogue of pafuramidine, in a monkey model of second stage human African trypanosomiasis. PLoS neglected tropical diseases. 2012; 6(7):e1734. [PubMed: 22848769]
18. Mdachi RE, Thuita JK, Kagira JM, Ngotho JM, Murilla GA, Ndung'u JM, Tidwell RR, Hall JE, Brun R. Efficacy of the novel diamidine compound 2,5-Bis(4-amidinophenyl)-furan-bis-O-Methlylamidoxime (Pafuramidine, DB289) against Trypanosoma brucei rhodesiense infection in vervet monkeys after oral administration. Antimicrob Agents Chemother. 2009; 53(3):953–957. [PubMed: 19064893]
19. Thuita JK, Wolf KK, Murilla GA, Liu Q, Mutuku JN, Chen Y, Bridges AS, Mdachi RE, Ismail MA, Ching S, Boykin DW, Hall JE, Tidwell RR, Paine MF, Brun R, Wang MZ. Safety, pharmacokinetic, and efficacy studies of oral DB868 in a first stage vervet monkey model of human African trypanosomiasis. PLoS neglected tropical diseases. 2013; 7(6):e2230. [PubMed: 23755309]

20. Ismail MA, Boykin DW. Synthesis of deuterium-labelled 6-[5-(4-amidinophenyl)furan-2-yl]nicotinamidine and N-alkoxy-6-{5-[4-(N-alkoxyamidino)phenyl]-furan-2-yl}-nicotinamidines. J Labelled Compd Rad. 2004; 47(4):233–242.

21. Kurian JR, Bajad SU, Miller JL, Chin NA, Trepanier LA. NADH cytochrome b5 reductase and cytochrome b5 catalyze the microsomal reduction of xenobiotic hydroxylamines and amidoximes in humans. J Pharmacol Exp Ther. 2004; 311(3):1171–1178. [PubMed: 15302896]

22. Paine MF, Schmiedlin-Ren P, Watkins PB. Cytochrome P-450 1A1 Expression in Human Small Bowel: Interindividual Variation and Inhibition by Ketoconazole. Drug Metab Dispos. 1999; 27(3):360–364. [PubMed: 10064566]

23. Shimada T, Yun CH, Yamazaki H, Gautier JC, Beaune PH, Guengerich FP. Characterization of human lung microsomal cytochrome P-450 1A1 and its role in the oxidation of chemical carcinogens. Mol Pharmacol. 1992; 41(5):856–864. [PubMed: 1588920]

24. Ishida K, Taguchi M, Akao T, Hashimoto Y. Involvement of the CYP1A subfamily in stereoselective metabolism of carvedilol in beta-naphthoflavone-treated Caco-2 cells. Biological & pharmaceutical bulletin. 2009; 32(3):513–516. [PubMed: 19252307]

25. Iwasaki K, Uno Y. Cynomolgus monkey CYPs: a comparison with human CYPs. Xenobiotica. 2009; 39(8):578–581. [PubMed: 19622000]

26. Nakanishi Y, Matsushita A, Matsuno K, Iwasaki K, Utoh M, Nakamura C, Uno Y. Regional distribution of cytochrome p450 mRNA expression in the liver and small intestine of cynomolgus monkeys. Drug metabolism and pharmacokinetics. 2010; 25(3):290–297. [PubMed: 20610888]

27. Ito S, Chen C, Satoh J, Yim S, Gonzalez FJ. Dietary phytochemicals regulate whole-body CYP1A1 expression through an arylhydrocarbon receptor nuclear translocator-dependent system in gut. J Clin Invest. 2007; 117(7):1940–1950. [PubMed: 17607366]

28. Keisu M, Andersson TB. Drug-induced liver injury in humans: the case of ximelagatran. Handbook of experimental pharmacology. 2010; (196):407–418. [PubMed: 20020269]

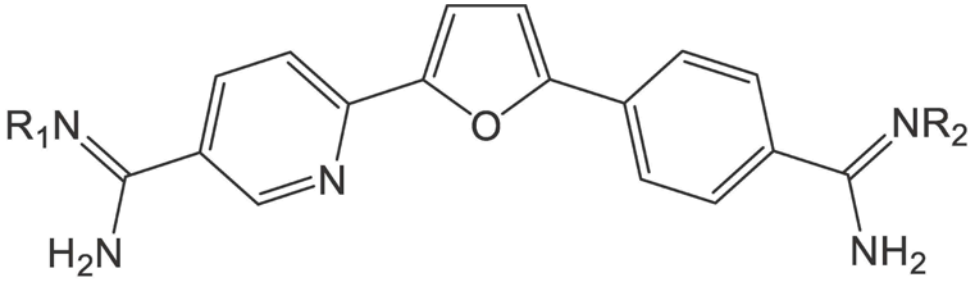

Name	R_1	R_2
DB844	OCH_3	OCH_3
M1A (DB1284)	OH	OCH_3
M1B (DB1058)	OCH_3	OH
M3 (DB821)	OH	OH
M2A (DB1285)	H	OCH_3
M2B (DB1212)	OCH_3	H
M4A	H	OH
M4B	OH	H
DB820	H	H
DB844-phenyl-CD_3	OCH_3	OCD_3
DB844-pyridyl-CD_3	OCD_3	OCH_3
DB844-D_4	OCH_3	OCH_3, deuterated phenyl

Figure 1.
Structures of DB844, DB820, intermediate metabolites, and deuterium-labeled DB844 analogs.

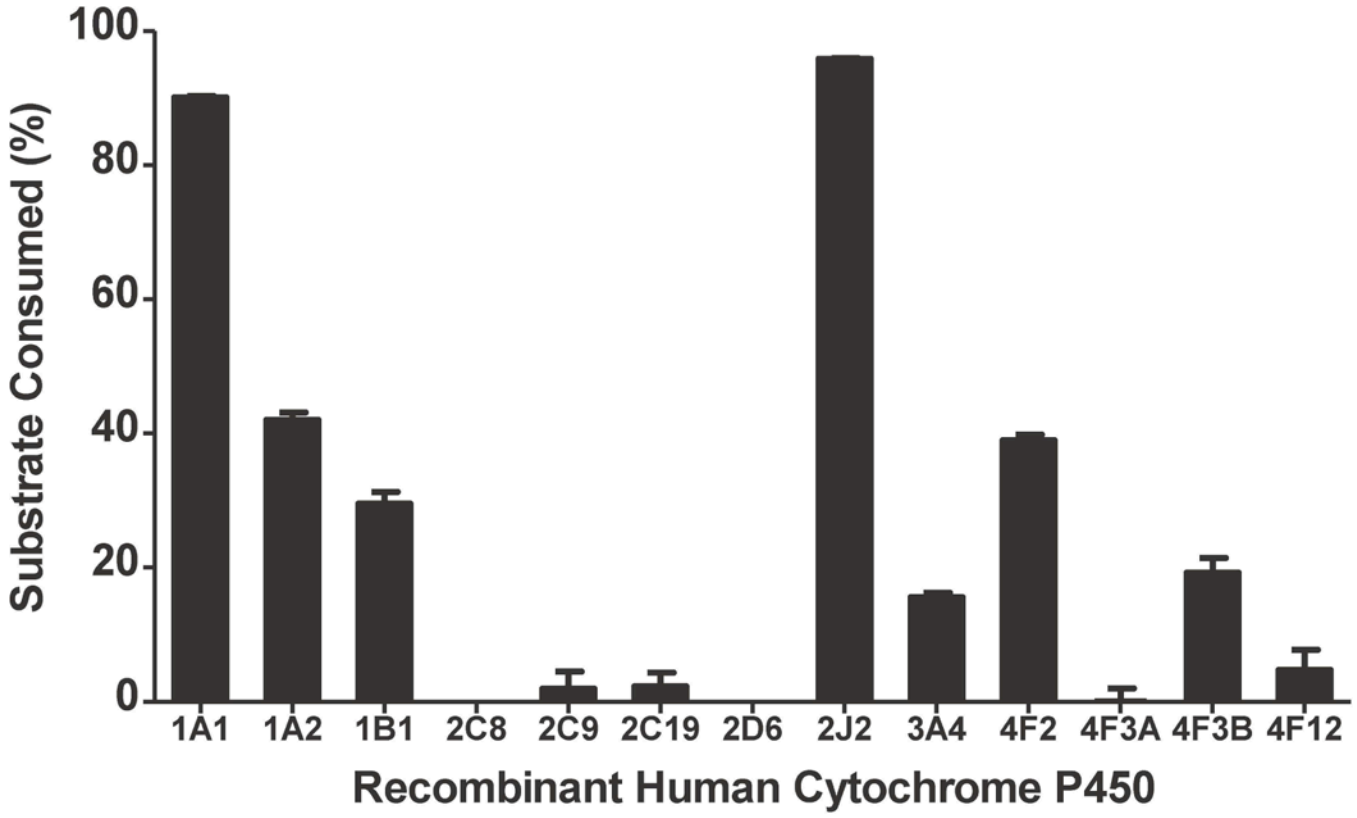

Figure 2. DB844 substrate depletion by recombinant human CYP enzymes

DB844 (3 μM) was incubated with 1 mM β-NADPH and either recombinant CYP enzymes individually (50 pmol/mL) or control Supersomes™ (0.25 mg/mL) for 15 min at 37°C. The percentage of DB844 consumed at the end of the reaction was determined by normalizing the DB844 concentration in recombinant CYP enzyme incubations to that with control Supersomes™ (expressed as 0%). Bars and error bars represent the means and standard errors, respectively, of triplicate determinations.

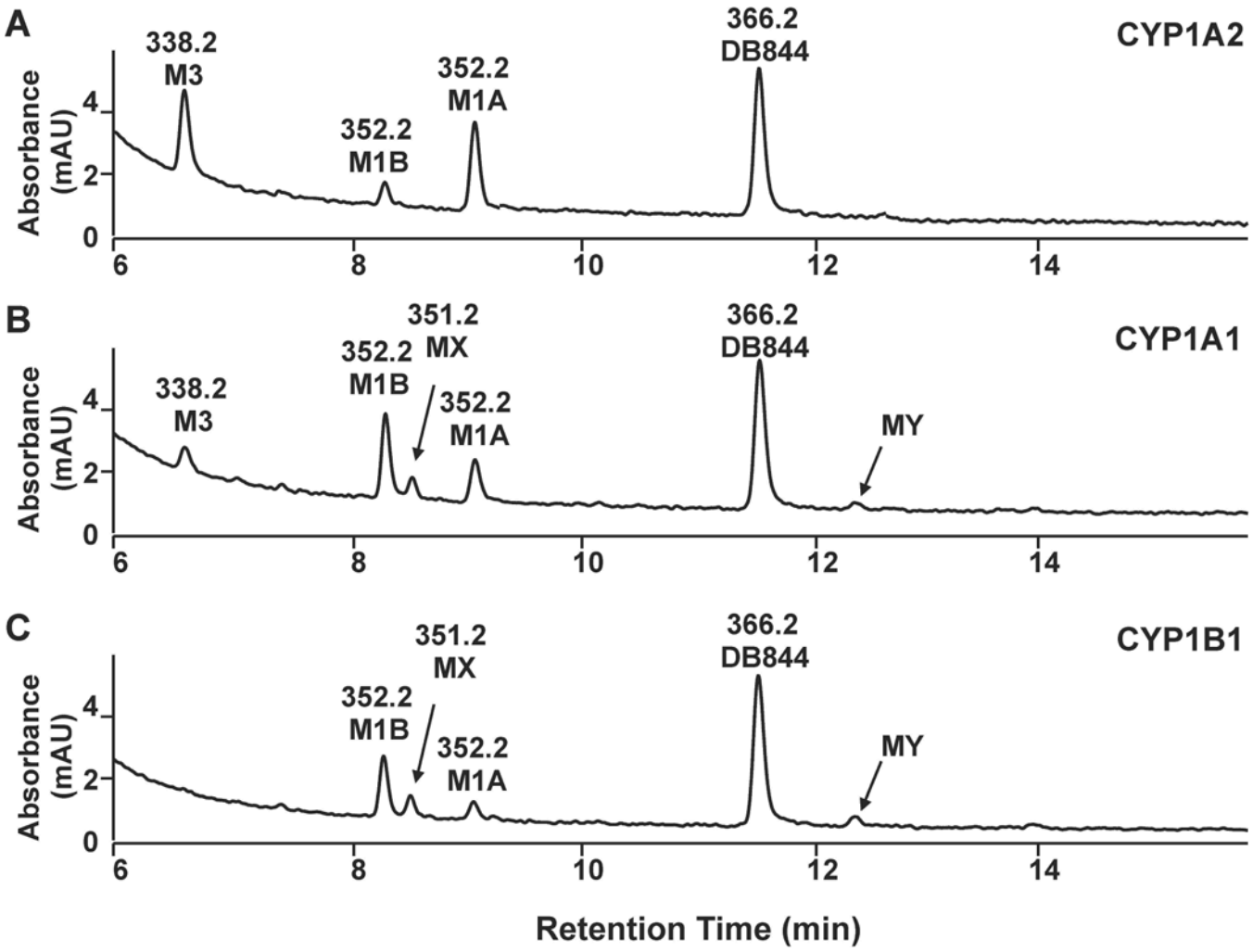

Figure 3. HPLC/UV chromatograms of DB844 incubated with recombinant human CYP1A2 (A), CYP1A1 (B), and CYP1B1 (C)

DB844 (3 μM) was incubated with 1 mM β-NADPH and either 50 pmol/mL CYP1A2 or CYP1B1, or 10 pmol/mL CYP1A1 for 15 min at 37°C. Quenched reaction mixtures were analyzed by HPLC/ion trap MS as described under *Materials and Methods*. M1A, M1B, and M3 were identified by comparing retention times and MS fragmentation patterns to those of authentic standards. The molecular ions ($[M+H]^+$; m/z) of DB844 and detected metabolites are indicated next to the corresponding HPLC/UV peaks.

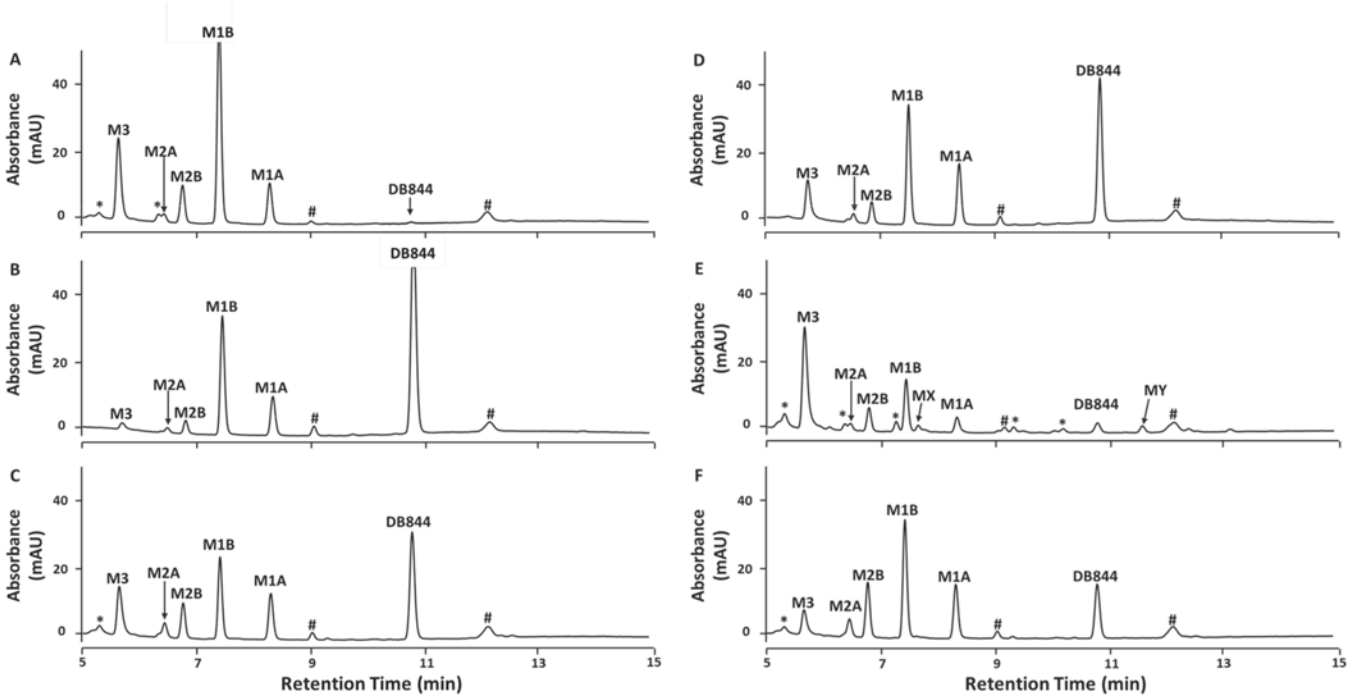

Figure 4. HPLC/UV chromatograms of DB844 incubated with pooled HLM (A), pooled HIM (B), vervet LM (C), vervet IM (D), cynoLM-β-NF (E) and cynoLM-saline (F)

DB844 (10 μM) was incubated with 1 mM β-NADPH and 1.0 mg/mL liver or intestinal microsomes for 30 min at 37°C. Quenched reaction mixtures were analyzed by HPLC/UV as described under *Materials and Methods*. *, unidentified metabolites; #, background peaks.

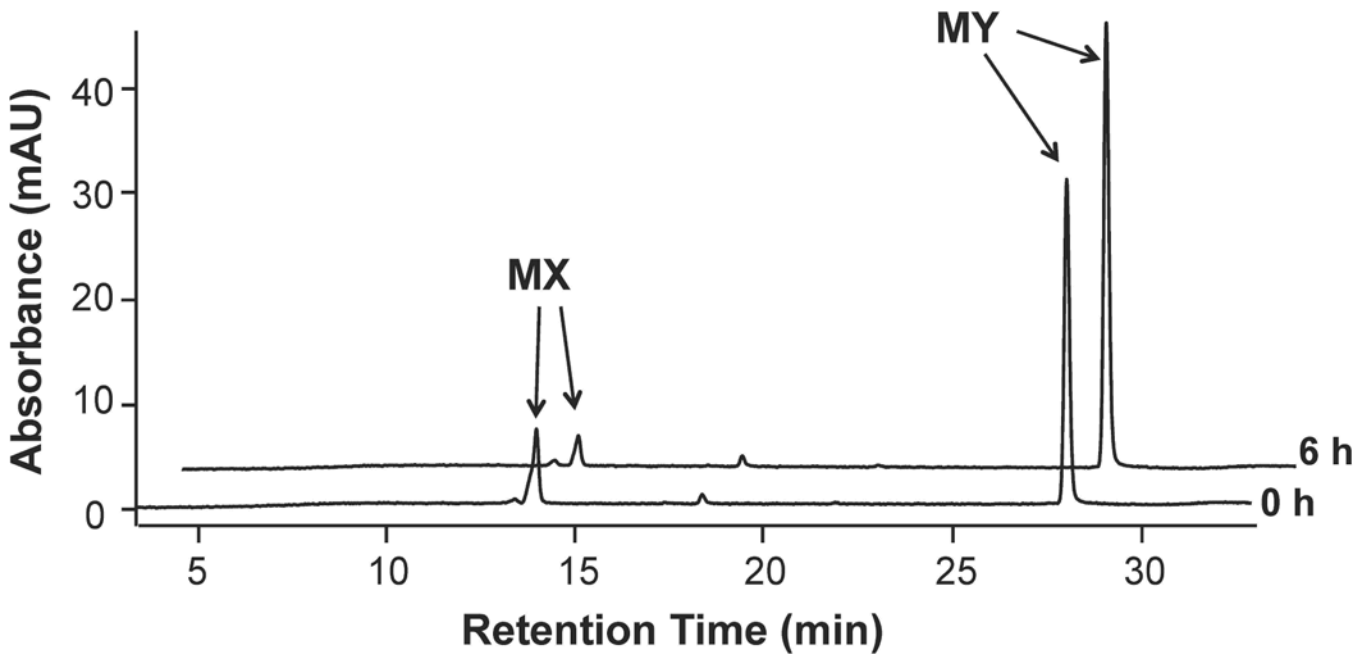

Figure 5. HPLC/UV chromatogram of biosynthesized MX after purification

MX was biosynthesized and purified as described under *Materials and Methods*. Purified MX was concentrated using an Empore C18-SD SPE cartridge, dried down, and reconstituted in 0.1 mL of 50% (v/v) acetonitrile. The reconstituted sample was immediately analyzed (0 h) by HPLC/UV or kept at room temperature for 6 h prior to analysis. Chromatograms are plotted on the same UV absorbance scale to facilitate the comparison of peak heights.

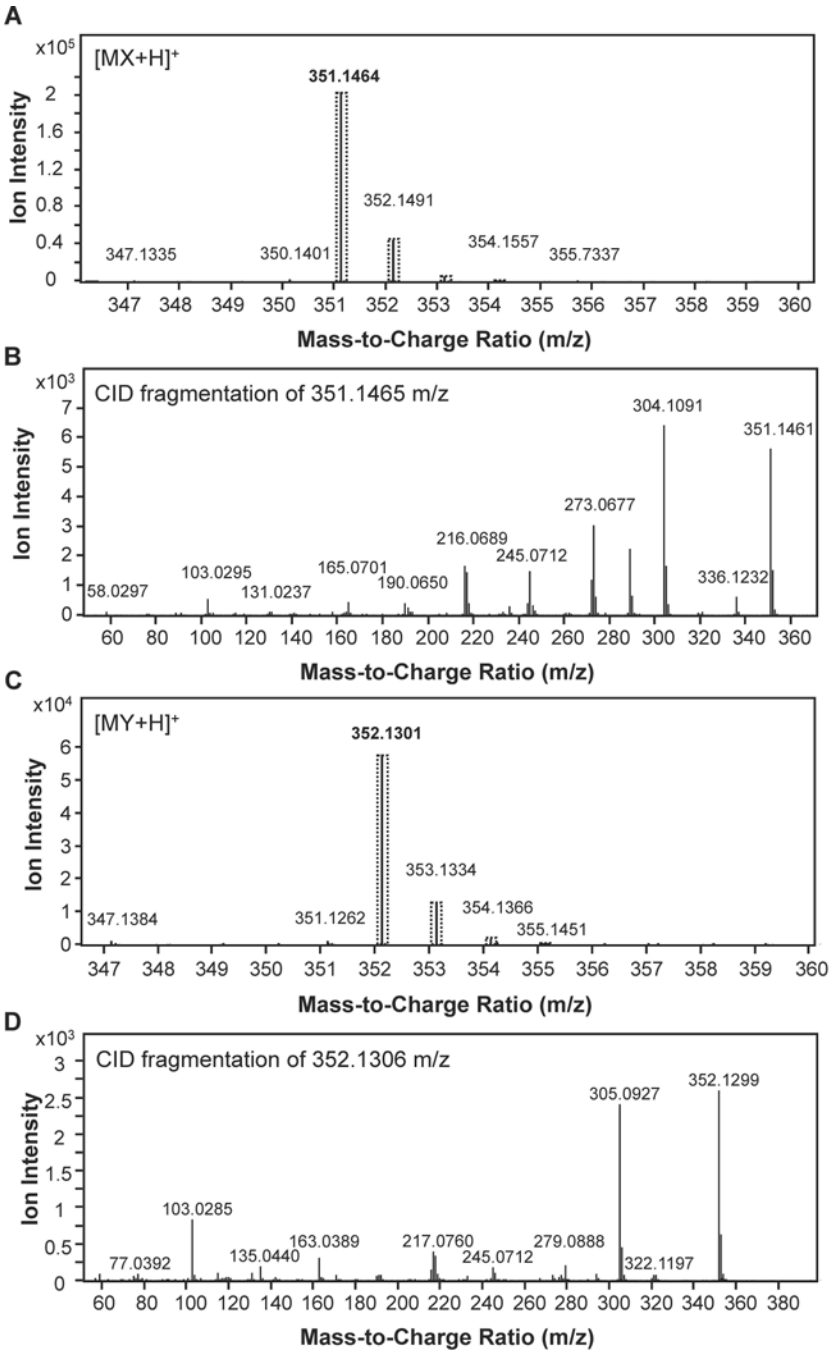

Figure 6. Accurate mass analysis of MX (A and B) and MY (C and D) by HPLC/Q-TOF

MX and MY were generated from incubations of DB844 (3 μM) with recombinant CYP1A1 (50 pmol/mL). Quenched reaction mixtures were separated on an analytical column prior to introduction into a high resolution Q-TOF mass spectrometer for MS full scan (A and C) and CID fragmentation analysis (B and D). Boxes with dotted lines denote the predicted isotopic abundance based on the assigned formula for MX ($C_{19}H_{18}N_4O_3$) and MY ($C_{19}H_{17}N_3O_4$), matching with the observed ion abundance of corresponding mass-to-charge ratio.

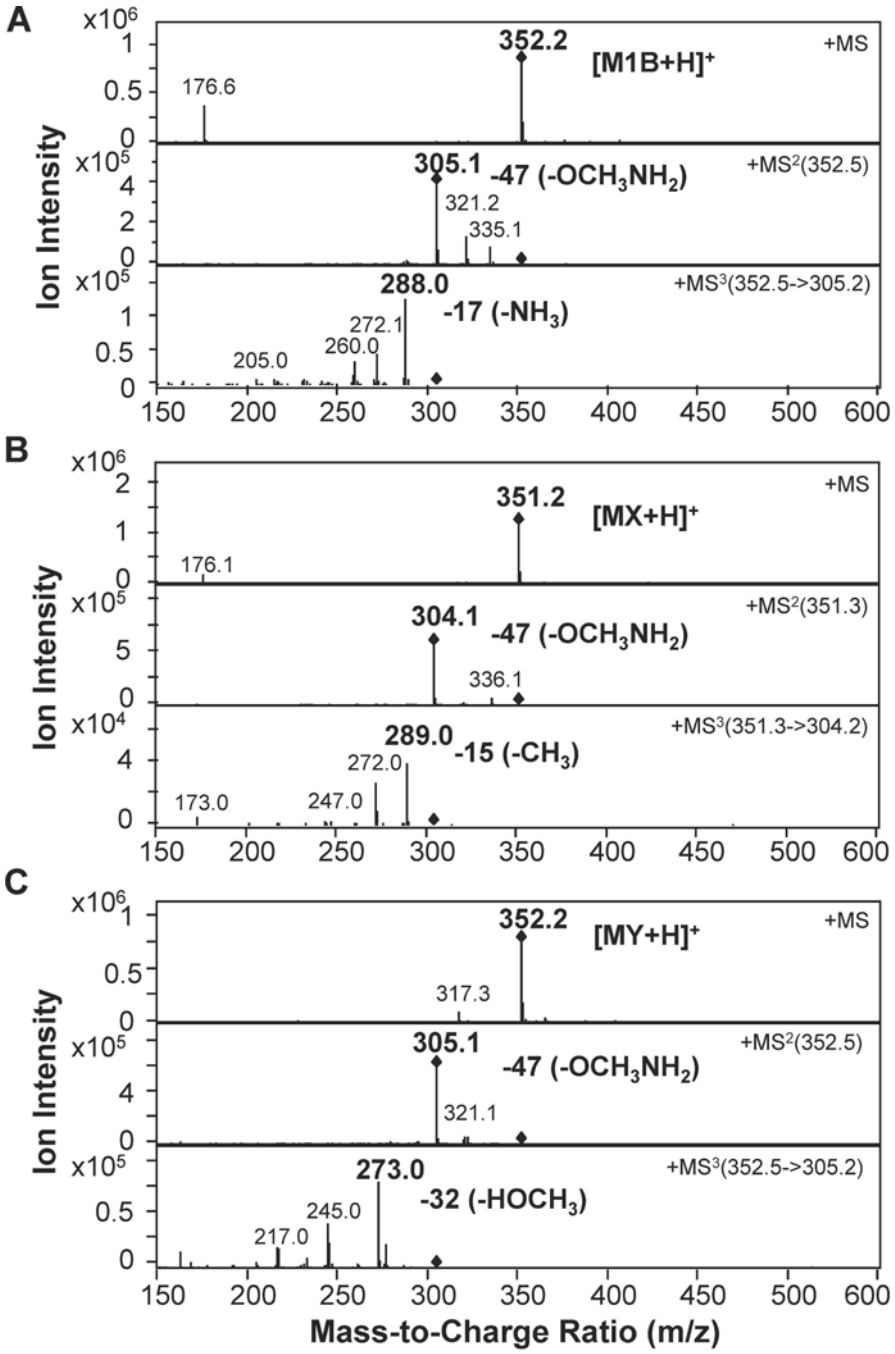

Figure 7. HPLC/ion trap MS analysis of authentic M1B standard (A) and biosynthesized MX (B) and MY (C)

Samples were separated on an analytical column prior to introduction into an electrospray interface and analysis by an ion trap MS to obtain MS full scan (top panel), MS^2 (middle panel) and MS^3 (bottom panel) CID fragmentation mass spectra. The molecular ions and the most intense product ions are denoted in bold. Ions that were selected for CID fragmentation are denoted by a diamond symbol. Characteristic mass losses upon fragmentation are provided, as are corresponding chemical formula for the proposed mass loss in parenthesis.

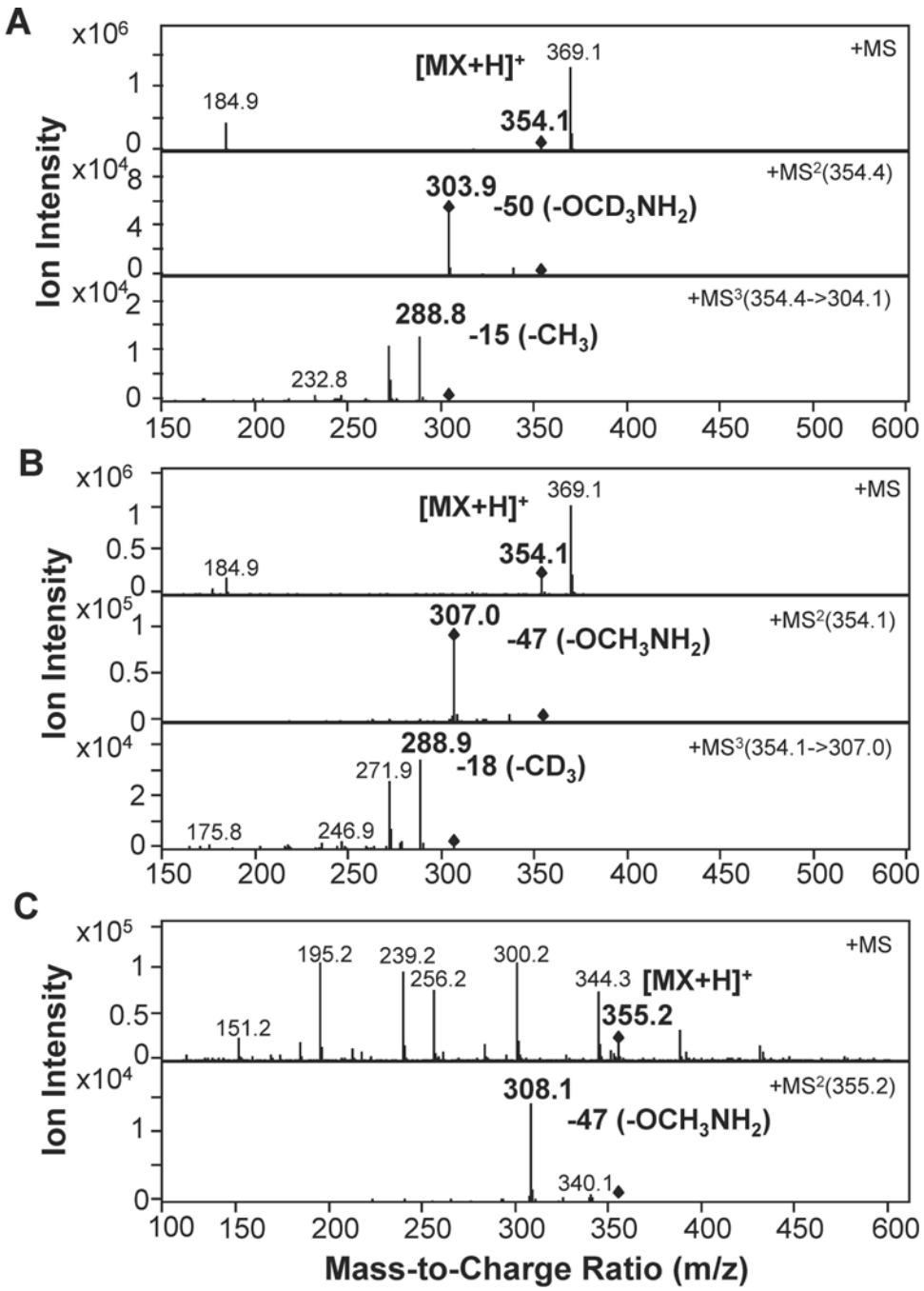

Figure 8. HPLC/ion trap MS analysis of MX formed from DB844-pyridyl-CD_3(A), DB844-phenyl-CD3 (B), or DB844-D_4(C)

Deuterium-labeled DB844 analogs (3 μM) were incubated with recombinant CYP1A1 (10 pmol/mL) for 15 min at 37°C. Quenched reaction mixtures were separated on an analytical column prior to introduction into an electrospray interface and analysis by an ion trap MS to obtain MS full scan (top panel), MS^2 (middle panel) and MS^3 (bottom panel) CID fragmentation mass spectra. The molecular ions and most intense product ions are denoted in bold. Ions that were selected for CID fragmentation are denoted by a diamond symbol. Characteristic mass losses upon fragmentation are provided, as are corresponding chemical formula for the proposed mass loss in parenthesis.

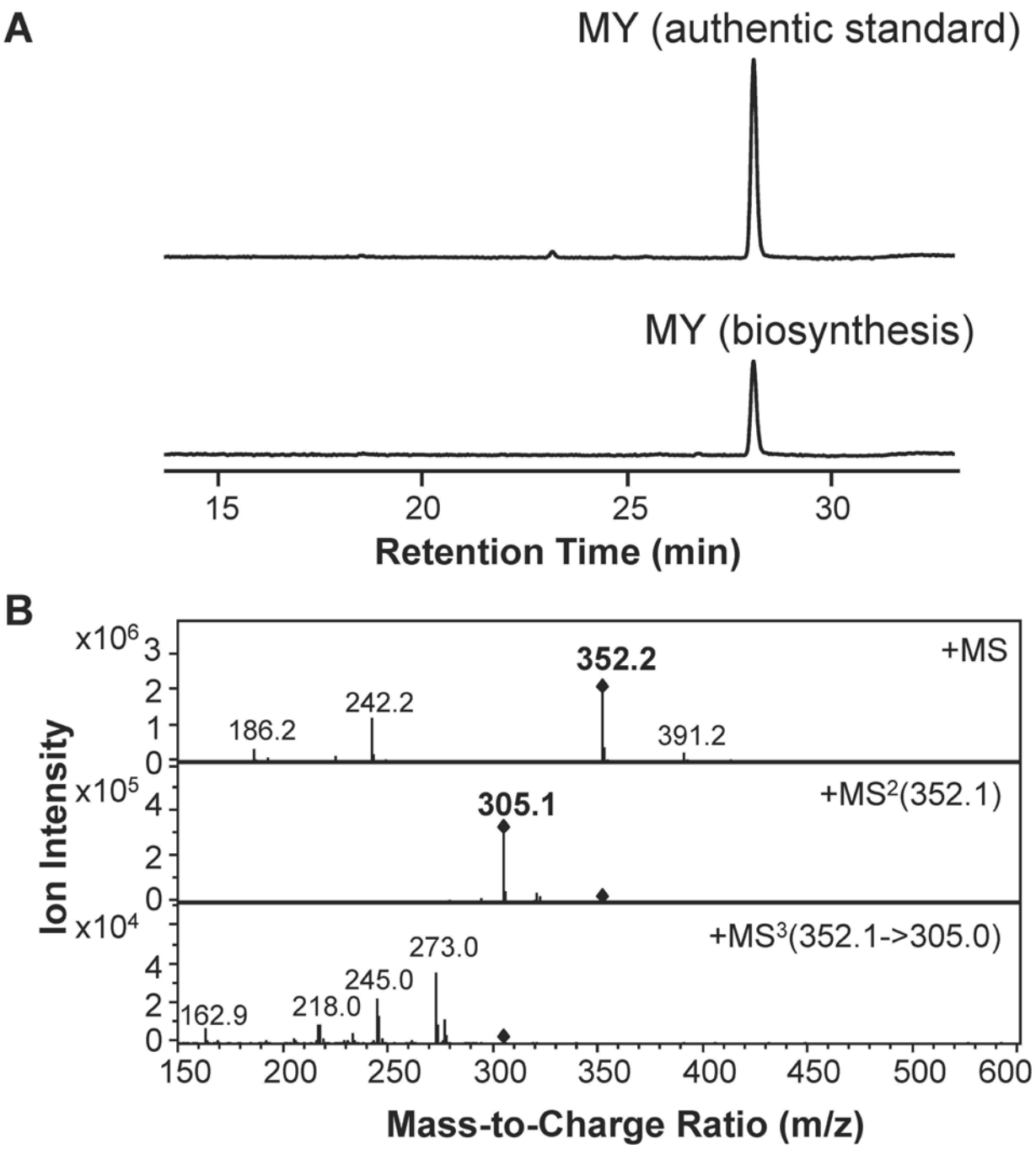

Figure 9. HPLC/UV and HPLC/ion trap MS analyses of chemically synthesized and biosynthesized MY

(A) HPLC/UV chromatograms of chemically synthesized (authentic standard; top panel) and biosynthesized (bottom panel) MY. **(B)** MS full scan (top panel), MS^2 (middle panel), and MS^3 (bottom panel) CID fragmentation mass spectra of chemically synthesized MY. Comparison of HPLC retention times and CID fragmentation patterns for synthetic MY and biosynthesized MY to those in Figure 6C support the proposed structure of MY.

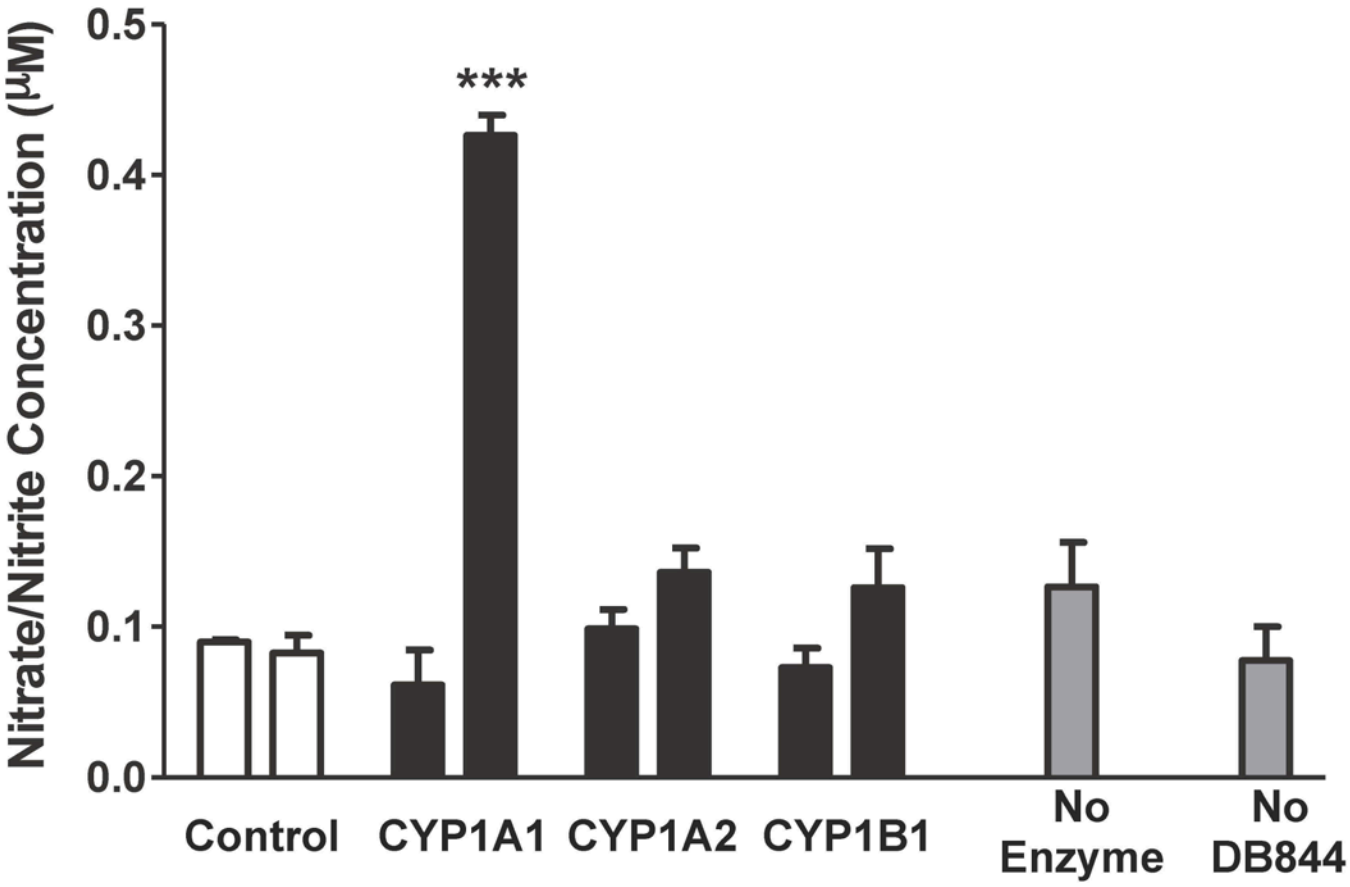

Figure 10. Nitric oxide formation in incubations of DB844 with recombinant human CYP enzymes

DB844 (10 μM) was incubated with 1 mM β-NADPH and either recombinant CYP1A1, CYP1A2, or CYP1B1 (50 pmol/mL) or control Supersomes (0.25 mg/mL) for 1 h. Nitric oxide formation was determined by measuring the total concentration of nitrate and nitrite present in each reaction mixture. Negative controls consisted of incubating DB844 with enzymes that had been heat-inactivated (90°C for 5 min). Incubations without enzyme (but with DB844 and β-NADPH) or without DB844 (but with CYP1A1 and β-NADPH) served as additional controls. The left bar of each pair represents nitric oxide formation in negative controls, while the right bar represents formation in incubations with active enzyme. Bars and error bars represent the means and standard errors, respectively, of triplicate determinations. Statistical differences in nitric oxide formation between negative controls and incubations with active enzymes were evaluated by unpaired, two-tailed Student's *t*-tests. ***, $p<0.001$, incubation with active *vs.* heat-inactivated CYP1A1.

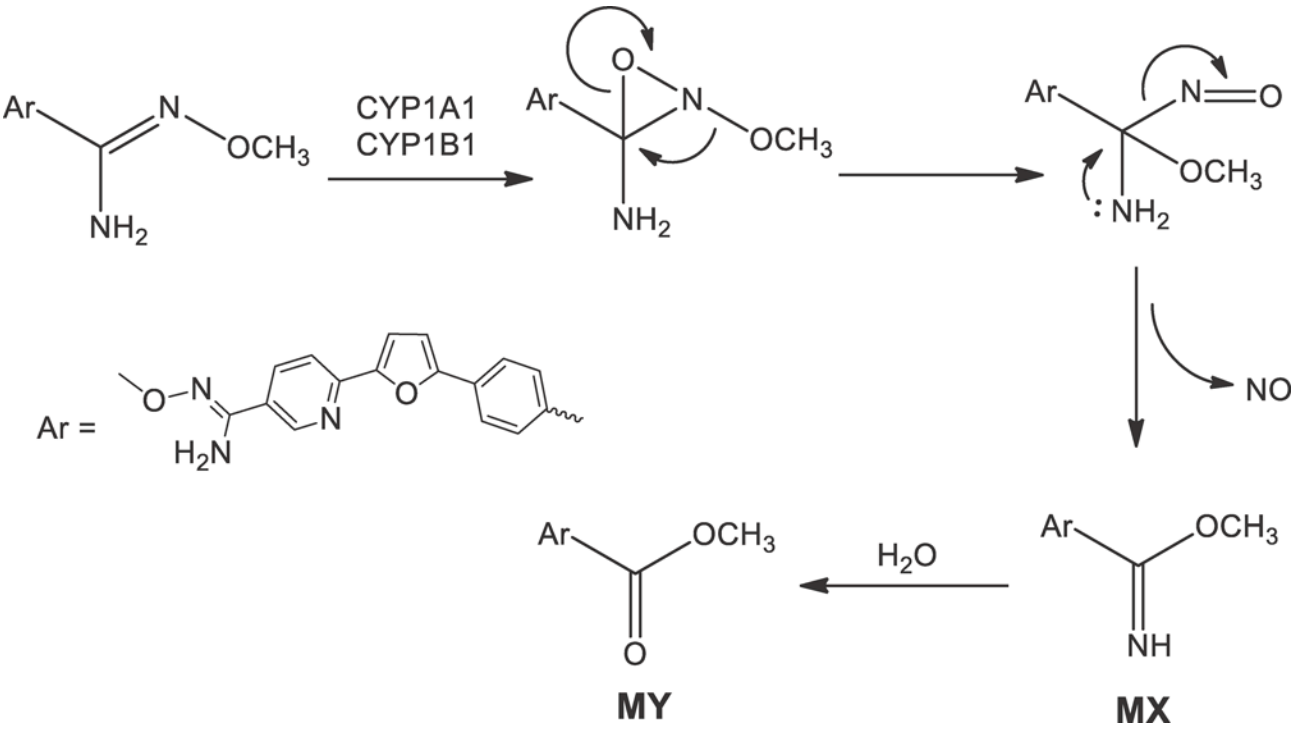

Scheme 1.
Proposed reaction mechanism of CYP1A1/1B1-mediated MX and MY formation from DB844: intramolecular rearrangement and release of nitric oxide.